https://doi.org/10.1016/j.energy.2016.06.128

Performance assessment of a hybrid system integrating a molten carbonate fuel cell and a thermoelectric generator

Sijie Wu [a], Houcheng Zhang[a, b*], Meng Ni [b]

[a] *Department of Microelectronic Science and Engineering, Ningbo University, Ningbo 315211, China*

[b] *Department of Building and Real Estate, The Hong Kong Polytechnic University, Hong Kong, China*

Abstract: A hybrid system consisting of an MCFC (Molten Carbonate Fuel Cell), a TEG (Thermoelectric Generator) and a regenerator is proposed and evaluated. In this system, the MCFC produces electricity and heat from fuels and the TEG utilizes the heat for additional power generation. A numerical model is developed to evaluate the performance of the proposed system. The relationship between the operating current density of the MCFC and the dimensionless current of the TEG is theoretically derived and the operating current density region of the MCFC that allows the TEG to function is determined. Numerical expressions of the power output and efficiency for the hybrid system are specified under different operating conditions. The general performance characteristics and optimum criteria for the hybrid system are revealed. It is found that the hybrid system is superior to the stand-alone MCFC system as the bottoming TEG can effectively increase the maximum power density. In addition, the effects of the operating current density, operating temperature, operating pressure, heat conductivity, integrated parameters and dimensional figure of merit on the performance characteristics of the hybrid system are investigated. The results obtained are useful for the design and optimization of novel MCFC system to achieve a better performance.

Keywords: Molten carbonate fuel cell; Thermoelectric generator; Hybrid system; Irreversible loss; Performance assessment

[*]Corresponding author. Tel.: +86 574 87600770; Fax: +86 574 87600744.

E-mail addresses: zhanghoucheng@nbu.edu.cn (H. Zhang).

1. Introduction

Due to their potentially lower greenhouse gas emissions and primary energy consumptions, fuel cells have been considered as next generation power sources to replace conventional thermal power technologies [1-7]. Based on electrolyte types, fuel cells can be classified into five major categories: proton exchange membrane fuel cell (PEMFC), alkaline fuel cell (AFC), phosphoric acid fuel cell (PAFC), solid oxide fuel cell (SOFC), and molten carbonate fuel cell (MCFC) [8]. Among the various fuel cells, MCFC is fuel flexible, long-term stable, and suitable for stationary applications [9-12]. The MCFC is a natural carbon capture system that enables to separate carbon dioxide from the original cathodic flow via the CO_3^{2-} transit through the electrolyte [13]. Unlike some carbon capture and storage technologies such as calcium looping [14, 15], the MCFC does not consume but provide power while operating as a CO_2 separator and concentrator [16]. Nowadays, MCFCs are commercially available in some countries such as USA, Germany, Japan, Italy and South Korea [17].

Although progress has been made in MCFCs to prolong the lifetime, improve the stack capacity and lower the manufacturing and running cost [18-20], the relatively low power density is still a major drawback that restricts the wide commercialization of MCFCs [21]. The power density of MCFC can be improved by optimizing the operating conditions or by developing more effective catalyst materials to reduce the activation loss. From engineering point of view, the MCFC performance can also be improved by recovering the waste heat released in MCFC for additional power generation or for combined heat and power (CHP) cogeneration [22-28]. Zhang et al. [22, 23] proposed two MCFC-gas turbine (MCFC-GT) hybrid systems with different fuels and investigated effects of some operating conditions and irreversible losses on the performance of the hybrid systems. Sánchez et al. [24] presented a reciprocating engine with three bottoming thermal cycles to recover

the waste heat from an MCFC and showed that the Stirling engine was an alternative choice for conventional gas turbines. Angelino et al. [25] considered an ORC (Organic Rankine Cycle) with different working fluids to recover the waste heat from an MCFC. The power and efficiency gain of about in the range 10 to 15% can be obtained with reference to MCFC plant in the capacity range of 2 to 5 MW. Baronci et al. [26] studied the integration of an MCFC and a Brayton cycle using supercritical carbon dioxide as working fluid. The boost in electrical efficiency was found to be twice that of a recovery system based on an ORC. Mamaghani et al. [27] proposed an MCFC-GT and ORC hybrid plant, 4E (energetic, exergetic, economic and environmental) analyses were performed and a multi-objective optimization method was utilized to build a set of Pareto optimal solutions. The optimum solutions showed that the exergetic efficiency of the MCFC-GT-ORC system was about 55%, about 5% larger than that of the sole MCFC-GT system. Silveira et al. [28] carried out energy, exergy and economic analyses of an MCFC integrated with an absorption refrigeration system for cold water production. A global efficiency of 86% and the payback period of about 3 and 5 years for investments in MCFCs of 1000 and 1500 US/kW were estimated.

Thermoelectric generators (TEGs) use thermal energy to create a temperature gradient across the hot and cold junctions of a thermoelectric material which is used to generate voltage as per the principle of Seebeck effect [29-31]. TEGs can be operated in a quiet way compared with other power generation technologies since TEGs are solid-state heat engine and do not contain any moving part. In addition, TEGs offer many other advantages such as compact, environmentally friendly, highly reliable and adapting to different kinds of heat reservoirs [32, 33]. Owing to these advantages, TEGs have drawn more and more attention for waste heat recovery [34-37]. With the rapid developments of thermoelectric materials, the working temperatures of some thermoelectric generators beyond

600 °C have already been reported [38-40]. It creates an opportunity to directly integrate a TEG with an MCFC for converting the waste heat into electricity to increase the power output and efficiency of the MCFC system.

In this work, a new hybrid system integrating an MCFC and a TEG is proposed to improve the energy efficiency for power generation. The layout of the hybrid system will be described and each component in the hybrid system will be numerically characterized. Some important parameters for assessing the performance of the hybrid system will be formulated by taking the main irreversible losses of the system into account. The general performance characteristics and optimum criteria for the hybrid system will be investigated and discussed. Effects of some designing parameters and operating conditions on the hybrid system performance will be specified. Some possible problems for the practical operation of the hybrid system are also discussed.

2. Model description

The hybrid system composed of an MCFC, a TEG and a regenerator, as schematically shown in Fig. 1 (a). The MCFC converts the chemical energy in reactants into electricity and waste heat, and the electricity is delivered to external loads. The waste heat, one part is transferred to the bottoming TEG for additional electricity generation, another part is used to compensate the regenerative losses in the regenerator, and the last part is dissipated into the environment. In Fig. 1 (a), P_{MCFC} stands for the electric power output of the MCFC, q_1 is the heat-transfer rate from the MCFC at temperature T to the hot junction of TEG at temperature T_1, q_2 is the heat-transfer rate from the cold junction of TEG at temperature T_2 to the environment at temperature T_0, P_{TEG} is the additional power output from the TEG, q_r is the heat-transfer rate from the MCFC to the regenerator, q_L is the heat-leak rate from the MCFC to the environment.

For simplification of analyses, the following assumptions are invoked [41-47]:

- Both the MCFC and the TEG are operated under steady state conditions;
- Operating temperature and pressure are uniform and constants in the MCFC;
- All reactants are all consumed in MCFC;
- Internal electric current through the electrolyte is neglected;
- Geometric configuration of the TEG is in the optimum form;
- Heat leakage from the TEG to the surroundings is neglected;
- Heat transfers within the system obey Newton's law;
- Electric current generated by the TEG flows along the arm of the device;
- TEG is closely attached to the MCFC, temperatures of the hot and cold junctions equal to that of the MCFC and the environment, respectively;
- Seebeck coefficient, electrical resistance, thermal conductance, and dimensional figure of merit of the TEG are independent of temperature.

2.1. The MCFC

The MCFC is a core element in the hybrid system, which simultaneously produces electricity and heat through electrochemical reactions. In the normal operation of MCFC, some other heat is also generated due to irreversible losses such as anode overpotential, cathode overpotential and ohmic overpotential. According to the theory of chemical thermodynamics [48] and the semi-empirical electrochemical model developed by Yuh and Selman [49], the power output P_{MCFC} and efficiency η_{MCFC} of an MCFC can be, respectively, expressed as

$$P_{MCFC} = jA(E - U_{an} - U_{cat} - U_{ohm}), \quad (1)$$

and

$$\eta_{MCFC} = \frac{n_e F}{-\Delta h}\left(E - U_{an} - U_{cat} - U_{ohm}\right), \tag{2}$$

where

$$E = E_0 + \frac{RT}{n_e F}\ln\left[\frac{p_{\mathrm{H_2,an}}\left(p_{\mathrm{O_2,cat}}\right)^{0.5} p_{\mathrm{CO_2,cat}}}{p_{\mathrm{H_2O,an}}\, p_{\mathrm{CO_2,an}}}\right], \tag{3}$$

$$E_0 = \left(242000 - 45.8T\right)/\left(n_e F\right), \tag{4}$$

$$U_{an} = 2.27\times10^{-9}\, j \exp\left(\frac{E_{act,an}}{RT}\right) p_{\mathrm{H_2,an}}^{-0.42} p_{\mathrm{CO_2,an}}^{-0.17} p_{\mathrm{H_2O,an}}^{-1.0}, \tag{5}$$

$$U_{cat} = 7.505\times10^{-10}\, j \exp\left(\frac{E_{act,cat}}{RT}\right) p_{\mathrm{O_2,cat}}^{-0.43} p_{\mathrm{CO_2,cat}}^{-0.09}, \tag{6}$$

$$U_{ohm} = 0.5\times10^{-4}\, j \exp\left[3016\left(\frac{1}{T} - \frac{1}{923}\right)\right], \tag{7}$$

where j is the operating current density; A is the effective polar plate area of the MCFC; E is the equilibrium potential, E_0 is the ideal standard potential; U_{an}, U_{cat} and U_{ohm} are, respectively, the anode overpotential, cathode overpotential, and ohmic overpotential; n_e is the number of electrons involved per reaction; F is Faraday's constant; R is the universal gas constant; T is the operating temperature; $E_{act,an}$ and $E_{act,cat}$ are, respectively, the anode and cathode activation energy; $p_{\mathrm{H_2}}$, $p_{\mathrm{O_2}}$, $p_{\mathrm{H_2O}}$, $p_{\mathrm{CO_2}}$ are, respectively, the partial pressures of H_2, O_2, H_2O and CO_2; Δh is the molar enthalpy change of the electrochemical reaction.

2.2. The TEG

The TEG in the hybrid system is operated between the hot reservoir (i.e., MCFC) and the heat sink (i.e., environment). The TEG is composed of many thermoelectric elements, as schematically shown in Fig. 1 (b). Each thermoelectric element is comprised of n-type and p-type semiconductor

legs that are connected electrically in series by metal strips and thermally in parallel. The thermoelectric elements are assumed to be insulated, both electrically and thermally, from their surroundings, except at the junction-reservoir contacts [50]. When the TEG operates stably, the boundary conditions are determined by $T_1(0)=T_2(0)=\cdots=T_i(0)=\cdots=T_m(0)=T$ and $T_1(L)=T_2(L)=\ \cdots=T_i(L)=\cdots=T_m(L)=T_0$, where L is the arm length of the generator, m is the number of thermoelectric elements. The internal irreversibilities inside the TEG are mainly caused by Joulean electrical resistive loss and heat conduction loss between hot and cold junctions. In addition to the internal irreversibilities, there also exist some external irreversibilities resulting from the finite rate heat transfer. Based on the theory of non-equilibrium thermodynamics, one can obtain the heat conductions between the TEG and the MCFC and the environment as follows [44, 51]:

$$q_1=\alpha I_g T-0.5I_g^2R+K(T-T_0), \tag{8}$$

and

$$q_2=\alpha I_g T_0+0.5I_g^2R+K(T-T_0), \tag{9}$$

where $\alpha=(\alpha_p+\alpha_n)m$ is the overall Seebeck coefficient, and the subscripts “p” and “n” denote p- and n-type semiconductors; I_g is the electrical current flows through the TEG, I_g^2R represents the Joule heat resulted from the electrical resistance, $R=(\rho_p l_p/S_p+\rho_n l_n/S_n)m$ is the overall electrical resistance, ρ is the electrical resistivity of the semiconductor materials, l and S are the length and cross-sectional area of the semiconductor arms; $K=(\kappa_p S_p/l_p+\kappa_n S_n/l_n)m$ is the overall thermal conductance, κ is the thermally conductivity of the semiconductor materials; and $K(T-T_0)$ represents the heat-leakage caused by the temperature difference between the hot and cold junctions.

Based on Eqs. (8) and (9), the power output P_{TEG} and efficiency η_{TEG} of the TEG can be, respectively, expressed as [44]

$$P_{TEG} = q_1 - q_2 = K(T - T_0)J - KJ^2 / Z , \tag{10}$$

and

$$\eta_{TEG} = \frac{P_{TEG}}{q_1} = \frac{Z(T - T_0)J - J^2}{Z(T - T_0) + ZTJ - J^2 / 2}, \tag{11}$$

where $J = \alpha I_g / K$ and $Z = \alpha^2 / (KR)$ are, respectively, the dimensionless current and the figure of merit of thermoelectric materials.

2.3. The regenerator

The regenerator in the hybrid system is an important auxiliary device that heats the inlet reactants from the ambient temperature T_0 to the MCFC operating temperature T by means of the high-temperature exhaust gases. Due to the irreversibility associated with heat transfer, some regenerative losses are inevitable. The rate of regenerative losses are often assumed to be proportional to the temperature gap between the MCFC and the environment [42, 52]

$$q_{re} = K_{re} A_{re} (1 - \varepsilon)(T - T_0), \tag{12}$$

where K_{re} is the heat-transfer coefficient of the regenerator, A_{re} is the corresponding heat-transfer area, and ε is the effectiveness of the regenerator.

2.4. The equivalent power output and efficiency of the hybrid system

The heat-leak rate q_L is assumed to be proportional to the temperature difference between the MCFC and the environment. According to the Newton's heat-transfer law and the first law of thermodynamics, q_L and q_1 can be, respectively, expressed as [42, 52]

$$q_L = \alpha_L A_L (T - T_0), \tag{13}$$

and

$$q_1 = -\Delta \dot{H} - P_{MCFC} - q_{re} - q_L = -\frac{A\Delta h}{n_e F}\left[(1-\eta_{MCFC})\, j - \frac{n_e F\,(c_1 + c_2)(T - T_0)}{-\Delta h}\right], \tag{14}$$

where α_L is the heat-leak coefficient, A_L is the heat-transfer area, $c_1 = [K_{re} A_{re}(1-\varepsilon)]/A$ and $c_2 = (\alpha_L A_L)/A$ are two integrated parameters which are associated with the heat transfer irreversibilities, effectiveness of the regenerator, surface areas of the regenerator and the MCFC, and polar plate area of the MCFC.

By considering the heat-leakage between the hot and cold junctions, the TEG in the hybrid system begins to exert its function only when the following condition is satisfied:

$$-\Delta \dot{H} - P_{MCFC} > q_{re} + q_L + K(T - T_0). \tag{15}$$

Substituting Eqs. (1), (2), (12) and (13) into Eq. (15), Eq. (15) can be further explicitly expressed as

$$j > j_C = \left[\frac{n_e F}{-\Delta h(1-\eta_{MCFC})}\right]\left[(c_1 + c_2)(T - T_0) + K(T - T_0)/A\right], \tag{16}$$

where j_C is the lower bound operating current density from which the TEG starts to work. When $j > j_C$, the relationship between the dimensionless current of the TEG, J, and the operating current density of the MCFC, j, is determined by the following equation:

$$J^2 - 2ZTJ - 2Z(T - T_0) + \frac{2ZA}{K}\left[\frac{-\Delta h}{n_e F}(1-\eta_{MCFC})\, j - (c_1 + c_2)(T - T_0)\right] = 0. \tag{17}$$

Combining the condition of $P_{TEG} \geq 0$ and Eq. (17), one may easily determine the maximum operating current density of the MCFC, j_M, from which the TEG stops working. Thus, the TEG does not operate in the entire operating current density region but only works in the following region

$$j_C < j < j_M. \tag{18}$$

Based on Eqs. (1), (2), (10) and (11), when $j_C < j < j_M$, the power output P and efficiency η of hybrid system can be, respectively, expressed as

$$P = P_{MCFC} + P_{TEG} = VjA + KT_0[(T/T_0 - 1)J - J^2/(ZT_0)], \tag{19}$$

and

$$\eta = \frac{P_{MCFC} + P_{TEG}}{-\Delta \dot{H}} = \eta_{MCFC} + \frac{n_e FKT_0[(T/T_0 - 1)J - J^2/(ZT_0)]}{-jA\Delta h}. \tag{20}$$

When $j \le j_C$ or $j \ge j_M$, the power output and efficiency of hybrid system equal to that of the stand-alone MCFC, i.e.,

$$P = P_{MCFC}, \tag{21}$$

and

$$\eta = \eta_{MCFC}. \tag{22}$$

3. General performance characteristics and optimum criteria

As described by the mathematical model in Sec. 2, the performance characteristics of the MCFC-TEG hybrid system not only depends on the parameters such as operating current density j, operating temperature T, operating pressure p and partial pressures of species (i.e., $p_{\mathrm{H_2}}$, $p_{\mathrm{O_2}}$, $p_{\mathrm{H_2O}}$ and $p_{\mathrm{CO_2}}$) of the MCFC, electrical resistance R, thermal conductance K, geometric parameters (i.e., l and S) and dimensional figure of merit ZT_0 of the TEG, but also depends on some parameters related to thermodynamic losses within the system (i.e., c_1 and c_2). Based on the parameters summarized in Table 1 [41, 46, 50, 52], parametric analyses are conducted to investigate the effects of these parameters on the performance of the hybrid system. The values of these parameters are taken as default ones unless they are specified otherwise.

The power densities and efficiencies of the MCFC, TEG and hybrid system are compared in Fig.

2. $P^*_{MCFC} = P_{MCFC} / A$, $P^*_{TEG} = P_{TEG} / A$, $P^* = P / A$ are, respectively, the corresponding power densities. $P^*_{MCFC,\max}$, $P^*_{TEG,\max}$ and $P^*_{\max}$ are, respectively, the maximum achievable power densities for the MCFC, TEG and the hybrid system. j_P and η_P are, respectively, the operating current density and efficiency of the hybrid system at $P^*_{\max}$. $j_{P,fc}$ and $\eta_{P,fc}$ are, respectively, the operating current density and efficiency of the MCFC at $P^*_{MCFC,\max}$. $j_{P,t}$ is the operating current density at $P^*_{TEG,\max}$. $j_{\eta,t}$ is the operating current density at the maximum efficiency of the TEG $\eta_{TEG,\max}$. P^*_C and η_C are, respectively, the power density and efficiency of the hybrid system at j_C, and j_S is the stagnation current density from which the MCFC cannot output electrical power any more. Fig. 2 shows the state of the hybrid system at $P^*_{\max}$ is always different from that of the MCFC at $P^*_{MCFC,\max}$ or TEG at $P^*_{TEG,\max}$. It is observed that P^* and η are equal to or larger than P^*_{MCFC} and η_{MCFC}. This fact clearly shows that it is effective to couple a TEG to an MCFC for performance enhancement. It can be also seen that both P^* and P^*_{MCFC} first increase and then decrease with j in the entire region, while P^*_{TEG} shares the same characteristics only in the region of $j_C < j < j_M$. Out of this region, the curves of $P^* \sim j$ and $\eta \sim j$ are overlapped with that of $P^*_{MCFC} \sim j$ and $\eta_{MCFC} \sim j$, respectively. As distinct from the trend of power density, η first rapidly decreases then somewhat increases and finally decreases as j increases, this is because the performance gain contributed by the TEG is larger than the decrease caused by the MCFC in the anterior portion of $j_C < j < j_M$. Moreover, η_{MCFC} decreases as j increases in the whole region of j, while η_{TEG} first increases and then decreases in the region of $j_C < j < j_M$. For the typical parameters given in Table 1, numerical calculations show that P^* attains its maximum $P^*_{\max}$, 2053.1 W m^{-2}, when $j = j_P = 3148.2\ \mathrm{A\,m^{-2}}$, while P^*_{MCFC} achieves its maximum $P^*_{MCFC,\max}$, 1516.7 W m^{-2}, when $j = j_{P,fc} = 3024.2\ \mathrm{A\,m^{-2}}$, and $P^*_{\max}$ is about 35.4% larger than $P^*_{MCFC,\max}$. Meanwhile, η_P and

$\eta_{P,fc}$ are, respectively, 50.9% and 39.2%, and η_P is about 29.8% larger than $\eta_{P,fc}$. For comparison purposes, maximum power density improvements of some MCFC-based hybrid systems with reference to the stand-alone MCFC are clearly shown in Fig. 3, where the bottoming thermal devices not only include TEG and TIG (Thermionic Generator) but also include Diesel, Brayton, Atkinson, Rankine and Stirling heat engines [24, 53, 54]. As shown in Fig. 3, the maximum power density improvement of the present hybrid system is smaller than that of the hybrid systems integrated with Diesel, Brayton and Atkinson heat engines [54], but it is larger than the improvements of the hybrid systems integrated with TIG, Rankine and Stirling heat engines under typical temperatures. Considering the factors such as maintenance cost and structural simplicity, TEG may be served a competitive candidate as the bottoming thermal device for MCFCs.

As indicated by Fig. 2, when the hybrid system operates in the region of $j > j_P$, a continuous increase in j not only lowers P^* but also lowers η. Considering both P^* and η, it could be concluded that the hybrid system should be operated in the following region

$$j_C < j \le j_P . \tag{23}$$

When the hybrid system is operated in the region of $j_C < j \le j_P$, P^* will increase as η decreases, and vice versa. From the thermo-economic optimization viewpoint (i.e., trade-off optimization between P^* and η for a manufactured hybrid system) [55, 56], the optimum regions for P^* and η are, respectively, determined by

$$P_C^* < P^* \le P_{\max}^* , \tag{24}$$

and

$$\eta_C > \eta \ge \eta_P . \tag{25}$$

4. Results and discussion

4.1. Effects of operating temperature T

The operating temperature T is an important operating condition that not only affects the performance of the MCFC and TEG but also affects the thermodynamic losses within the hybrid system. As shown in Fig. 4, both P^* and η increase as T increases, and this effects become more significant with increasing T. At a larger T, the ionic conductivity in the electrolyte is more efficient and the electrodes are more reactive, which leads to smaller overpotential losses and a larger cell voltage, and thus, better performance of the MCFC can be achieved. In addition, a larger T creates a larger temperature gap between the hot junction and the cold junction, which also improves the performance of the TEG. As described by Eqs. (12) - (14), a larger T also leads to larger thermodynamic losses which reduce the amount of heat transferred from the MCFC to the TEG. Since the performance enhancements in the MCFC and TEG are more significant than the performance reduction from the thermodynamic losses, a larger T is always preferable. The values of j_P, j_C, j_M, j_S and Δj $(= j_M - j_C)$ increase as T increases. In practice, one should simultaneously consider the investment cost and the deterioration issue involved in manufacturing both a stack with the required thermal stability as well as the whole system that can be worked at that specific temperature.

4.2. Effects of operating pressure p

The operating pressure p not only affects the equilibrium potential but also affects the anode and cathode overpotentials. Fig. 5 shows that P^* and η increase with increasing p. The equilibrium potential increases as p increases, while the anode and cathode overpotentials decrease

with increasing p. The amount of the decrease in the overpotentials is less than that of the increase in the equilibrium potential, and consequently, the performance of the MCFC is improved with the increasing p. The effects of p on the performance become more significant at larger current densities. The values of $P^*_{\max}$, $P^*_{MCFC,\max}$, j_P, $j_{P,fc}$, j_C, j_M, j_S, Δj and Δj_P $(=\left|j_P - j_{P,fc}\right|)$ increase with increasing p. Generally, a larger operating pressure is more favorable for performance improvement, but it also costs more electricity to compress the inlet reactants, and thus 1 atm is usually used in practice. The black solid lines in Fig. 5 represent a common case where the operating pressure is 1 atm.

4.3. Effects of thermal conductance K

Different from the effects of T and p, the thermal conductance K only affects the system performance in the region of $j_C < j < j_M$, as shown in Fig. 6. Out of this region, the curves of $P^* \sim j$ and $\eta \sim j$ are overlapped with that of the $P^*_{MCFC} \sim j$ and $\eta_{MCFC} \sim j$, respectively. The values of j_P, j_C, j_M, Δj and Δj_P increase as K increases, while the values $j_{P,fc}$ and j_S keep invariants with the increasing K. P^*_{TEG} and η_{TEG} increase as K increases, however, only when K is large enough to make $j_M > j_{P,fc}$, the advantage of the hybrid system become an able competitor. When $j_M > j_{P,fc}$, the value of $P^*_{\max}$ first increases and then decreases as K increases. This is because the increase in P^*_{TEG} contributed by the TEG is less than the decrease in P^*_{MCFC} caused by the MCFC at large current densities and large thermal conductance. For the typical parameters given in Table 1, the optimum value of K is found to be between 0.03 W K^{-1} m^{-1} and 0.05 W K^{-1} m^{-1}. It is interesting to note from Fig. 6 that P^* and η can be still larger than zero even when $j > j_S$. In this situation, the MCFC is functioned as an isothermal heat reservoir of the

bottoming TEG rather than as an electrochemical converter. However, the larger K also demands higher requirement for materials fabrication, which often lead to higher manufacture cost.

4.4. Effects of integrated parameters c_1 and/or c_2

As indicated by Eqs. (14) - (17), the thermodynamic losses within the hybrid system are not only related to the operating temperature but also related to the integrated parameters c_1 and/or c_2. Similar to the effects of thermal conductance K, the effects of the integrated parameters c_1 and/or c_2 only occur in the region of $j_C < j < j_M$, and $P^* = P^*_{MCFC}$ and $\eta = \eta_{MCFC}$ are valid out of this region, as shown in Fig. 7. The peak values of the power density decrease as c_1 and/or c_2 are increased, while the current densities j_C, j_M, j_P and Δj increase as the parameter c_1 and/or c_2 are increased. The black solid lines in Fig. 7 represent a special case where both the regenerative losses in the regenerator and the heat leakage from the MCFC to the environment are negligible (i.e., $c_1 = c_2 = 0$). In this case, the fundamental relationship between j and J is reduced from Eq. (17) to

$$J^2 - 2ZTJ - 2Z(T - T_0) + \frac{2ZA}{K}\left[\frac{-\Delta h}{n_e F}(1-\eta_{MCFC})\, j\right] = 0 \tag{26}$$

4.5. Effects of dimensional figure of merit ZT_0

The dimensional figure of merit of the thermoelectric materials ZT_0 dramatically affects the power density and efficiency of the TEG and thus affects the performance of the hybrid system. With the rapid development of thermoelectric materials, some thermoelectric materials with the thermoelectric figure of merit larger than unity have been reported [57, 58], thus it is meaningful to discuss the effects of ZT_0 on the performance of the hybrid system. As shown in Fig. 8, both the

power density and the efficiency are increased with the increasing ZT_0. The effects of ZT_0 only occur in region of $j_C < j < j_M$, the values of $P_{\max}^*$ and j_P shift to larger ones as ZT_0 increases, while the values of j_C, j_M, j_S and Δj keep invariants as ZT_0 increases. To achieve a larger ZT_0, efforts can be made to increase the Seebeck coefficient α and decrease the electrical resistance R and the thermal conductance K simultaneously.

5. Conclusions

An MCFC-TEG hybrid system is presented to effectively harvest the waste heat released from the MCFC. The operating current density interval of the MCFC enables the TEG to exert its function is determined. Numerical expressions of two important parameters for assessing performance of the hybrid system are specified under different conditions. The maximum power density and the corresponding efficiency of the hybrid system allow over 30% larger than that of the stand-alone MCFC. Comparisons between the proposed system and some other MCFC-based hybrid systems in the literatures are carried out and the advantages of the present system are demonstrated. The optimum operating regions for performance parameters are determined by thermo-economic optimization approach. The effects of the operating current density, operating temperature, and operating pressure of the MCFC, thermal conductance of the TEG, dimensional figure of merit of thermoelectric materials and some integrated parameters related to the thermodynamic losses on the performance of the hybrid system are revealed. The results in the paper may alternatively provide some theoretical bases for the performance improvement of an MCFC through solid state cogeneration systems.

Acknowledgments

This work has been supported by the National Natural Science Foundation of China (Grant No. 51406091) , the K. C. Wong Magna Fund in Ningbo University, and The Hong Kong Polytechnic University Research Project (Grant No. 1-YW1F).

References

[1] Giddey S, Badwal SPS, Kulkarni A, Munnings C. A comprehensive review of direct carbon fuel cell technology. Prog Energy Comb Sci 2012;38:360-99.

[2] Dodds PE, Staffell I, Hawkes AD, Li F, Grunewwald P, McDowall W, Ekins P. Hydrogen and fuel cell technologies for heating: A review. Int J Hydrogen Energy 2015;40:2065-83.

[3] Mekhilef S, Saidur R, Safari A. Comparative study of different fuel cell technologies. Renew Sust Energy Rev 2012;16:981-9.

[4] Carton JG, Olabi AG. Three-dimensional proton exchange membrane fuel cell model: Comparison of double channel and open pore cellular foam flow plates. Energy 2016; http://dx.doi.org/10.1016/j.energy.2016.02.010.

[5] Carton JG, Lawlor V, Olabi AG, Hochenauer C, Zauner G. Water droplet accumulation and motion in PEM (Proton Exchange Membrane) fuel cell mini-channels. Energy 2012;39:63-73.

[6] Bruni G, Cordiner S, Mulone V. Domestic distributed power generation: Effect of sizing and energy management strategy on the environment efficiency of a photovoltaic-battery-fuel cell system. Energy 2014; 77:133-43.

[7] Cordiner S, Feola M, Mulone V, Romanelli F. Analysis of a SOFC energy generation system fuelled with biomass reformate. Appl Therm Eng 2007;27:738-47.

[8] Sharaf OZ, Orhan MF. An overview of fuel cell technology: Fundamental and applications. Renew Sust Energy Rev 2014;32:810-53.

[9] Ramandi MY, Berg P, Dincer I. Three-dimensional modeling of polarization characteristics in molten carbonate fuel cells using peroxide and superoxide mechanisms. J Power Sources 2012;218:192-203.

[10] Antolini E. The stability of molten carbonate fuel cell electrodes: A review of recent improvements. Appl Energy 2011;88:4274-93.

[11] Dicks AL. Molten carbonate fuel cells. Curr Opin Solid State Mater Sci 2004; 8:379-83.

[12] Brouwer J, Jabbari F, Leal EM, Orr T. Analysis of a molten carbonate fuel cell: Numerical modeling and experimental validation. J Power Sources 2006;158:213-24.

[13] Discepoli G, Cinti G, Desideri U, Penchini D, Proietti S. Carbon capture with molten carbonate fuel cells: Experimental tests and fuel cell performance assessment. Int J Greenh Gas Control 2012;9:372-84.

[14] Yin J, Qin C, An H, Veeraragavan A, Feng B. Influence of hydrogen by steam/superheating on the CO_2 capture performance and physical properties of CaO-based particles. Ind Eng Chem Res 2013;52:18215-24.

[15] Yin J, Kang X, Qin C, Feng B, Veeraragavan A, Saulov D. Modeling of $CaCO_3$ decomposition under CO_2/H_2O atmosphere in calcium looping processes. Fuel Process Technol 2014;125:125-38.

[16] Wee JH. Carbon dioxide emission reduction using molten carbonate fuel cell systems. Renew Sust Energy Rev 2014;32:178-91.

[17] Hu L, Rexed I, Lindbergh G, Lagergren C. Electrochemical performance of reversible molten carbonate fuel cells. Int J Hydrogen Energy 2014;39:12323-29.

[18] Donado RA, Marianowski LG, Maru HC, Selman JR. Corrosion of the wet-seal area in molten carbonate fuel cells I. Analysis. J Electrochem Soc 1984;131:2535-40.

[19] Freni S, Cavallaro S, Aquino M, Ravida D, Giordano N. Lifetime-limiting factors for a molten carbonate fuel cell. Int J Hydrogen Energy 1994;19:337-41.

[20] Bischoff M, Huppmann G. Operating experience with a 250 kW_{el} molten carbonate fuel cell (MCFC) power plant. J Power Sources 2002;105:216-21.

[21] Ramandi MY, Dincer I. Thermodynamic performance analysis of a molten carbonate fuel cell at very high current densities. J Power Sources 2011;196:8509-18.

[22] Zhang X, Guo J, Chen J. Influence of multiple irreversible losses on the performance of a molten carbonate fuel cell-gas turbine hybrid system. Int J Hydrogen Energy 2012;37:8664-71.

[23] Zhang X, Liu H, Ni M, Chen J. Performance evaluation and parametric optimum design of a syngas molten carbonate fuel cell and gas turbine hybrid system. Renew Energy 2015;80:407-14.

[24] Sánchez D, Chacartegui R, Torres M, Sánchez T. Stirling based fuel cell hybrid systems: An alternative for molten carbonate fuel cells. J Power Sources 2009;192:84-93.

[25] Angelino G, Paliano PC. Organic Rankine cycles (ORCs) for energy recovery from molten carbonate fuel cells. (IECEC) 35th Intersociety Energy Conversion Engineering Conference and Exhibit, Las Vegas, NV, 2000, pp. 1400-9.

[26] Baronci A, Messina G, McPhail SJ, Moreno A. Numerical investigation of a MCFC (Molten Carbonate Fuel Cell) system hybridized with a supercritical CO_2 Brayton cycle and compared with a bottoming Organic Rankine Cycle. Energy 2015;93:1063-73.

[27] Mamaghani AH, Najafi B, Shirazi A, Rinaldi F. 4E analysis and multi-objective optimization of an integrated MCFC (molten carbonate fuel cell) and ORC system. Energy 2015;82:650-63.

[28] Silveira JL, Leal EM, Ragonha Jr LF. Analysis of a molten carbonate fuel cell: cogeneration to produce electricity and cold water. Energy 2001;26:891-904.

[29] Chen WH, Wang CC, Hung CI, Yang CC, Juang RC. Modeling and simulation for the design of

thermal-concentrated solar thermoelectric generator. Energy 2014; 64:287-97.

[30] Yu S, Du Q, Diao H, Shu G, Jiao K. Start-up modes of thermoelectric generator based on vehicle exhaust waste heat recovery. Appl Energy 2015;138:276-90.

[31] Karri MA, Thacher EF, Helenbrook BT. Exhaust energy conversion by thermoelectric generator: Two case studies. Energy Convers Manag 2011;52:1596-1611.

[32] Qiu K, Hayden ACS. A natural-gas-fired thermoelectric power generation system. J Electron Mater 2009; 38:1315-9.

[33] Manikandan S, Kaushik SC. The influence of Thomson effect in the performance optimization of a two stage thermoelectric generator. Energy 100;227-37.

[34] Gou X, Yang S, Xiao H, Ou Q. A dynamic model for thermoelectric generator applied in waste heat recovery. Energy 2013;52:201-9.

[35] Hsiao YY, Chang WC, Chen SL. A mathematic model of thermoelectric module with applications on waste heat recovery from automobile engine. Energy 2010; 35:1447-54.

[36] Saidur R, Rezaei M, Muzammil WK, Hassan MH, Paria S, Hasanuzzaman M. Technologies to recover exhaust heat from internal combustion engines. Renew Sustain Energy Rev 2012; 16:5649-59.

[37] Lin J, Liao T, Lin B. Performance analysis and load matching of a photovoltaic-thermoelectric hybrid system. Energy Convers Manag 2015; 105:891-9.

[38] Pereira A, Caroff T, Lorin G, Baffie T, Romanjek K, Vesin S. High temperature solar thermoelectric generator – Indoor characterization method and modeling. Energy 2015;84:485-92.

[39] Baranowski L, Snyder G, Toberer S. Concentrated solar thermoelectric generators. Energy

Environ Sci 2012;5:9055-67.

[40] Candadai AA, Kumar VP, Barshilia HC. Performance evaluation of a natural convective-cooled concentration solar thermoelectric generator coupled with a spectrally selective high temperature absorber coating. Sol Energy Mater Sol Cells 2016;145:333-41.

[41] Zhang H, Lin G, Chen J. Performance analysis and multi-objective optimization of a new molten carbonate fuel cell system. Int J Hydrogen Energy 2011;36:4015-21.

[42] Zhang H, Lin G, Chen J. Performance evaluation and parametric optimum criteria of an irreversible molten carbonate fuel cell-heat engine hybrid system. Int J Electrichem Sci 2011; 6:4714-29.

[43] Chen L, Zhang H, Gao S, Yan H. Performance optimum analysis of an irreversible molten carbonate fuel cell-Stirling heat engine hybrid system. Energy 2014;64:923-30.

[44] Chen X, Pan Y, Chen J. Performance and evaluation of a fuel cell-thermoelectric generator hybrid system. Fuel Cells 2010; 10:1164-70.

[45] Chen X, Chen L, Guo J, Chen J. An available method exploiting the waste heat in a proton exchange membrane fuel cell system. Int J Hydrogen Energy 2011;36:6099-104.

[46] Chen J, Lin B, Wang H, Lin G. Optimal design of a multi-couple thermoelectric generator. Semicond Sci Technol 2000;15:184-8.

[47] Holman JP. Thermodynamics, 3rd Edition, McGraw-Hill, New York, 1980.

[48] Brian Smith E. Basic Chemical Thermodynamics, 5th Edition, Imperial College Press, London, 2004.

[49] Yuh CY, Selman JR. The polarization of molten carbonate fuel cell electrodes: I. Analysis of steady-state polarization data. J Electrochem Soc 1991;138:3642-8.

[50] Chen L, Sun F, Wu C. Thermodynamic-generator with linear phenomenological heat-transfer law. Appl Energy 2005;81:358-64.

[51] Chen J. Thermodynamic analysis of a solar-driven thermoelectric generator. J Appl Phys 1996; 79:2717-21.

[52] Zhao M, Zhang H, Hu Z, Zhang Z, Zhang J. Performance characteristics of a direct carbon fuel cell/thermoelectric hybrid system. Energy Conv Manag 2015;89:683-9.

[53] Huang C, Pan Y, Wang Y, Su G, Chen J. An efficient hybrid system using a thermionic generator to harvest waste heat from a reforming molten carbonate fuel cell. Energy Convers Manag 2016;121:186-93.

[54] Zhang X, Wang Y, Guo J, Shih TM, Chen J. A unified model of high-temperature fuel-cell heat-engine hybrid systems and analyses of its optimum performances. Int J Hydrogen Energy 2014;39:1811-25.

[55] Marechal F, Palazzi F, Godat J, Favrat D. Thermo-economic modeling and optimization of fuel cell systems. Fuel Cells 2005;5:5-24.

[56] Cheddie DF. Thermo-economic optimization of an indirectly coupled solid oxide fuel cell/gas turbine hybrid power plant. Int J Hydrogen Energy 2011;36:1702-9.

[57] Venkatasubramanian R, Siivola E, Colpitts T, O'Quinn B. Thin-film thermoelectric devices with high room temperature figures of merit. Nature 2001;413:597-602.

[58] Jovanovic V, Ghamaty S, Bass JC. New thermoelectric materials and applications. 13th IEEE Intersociety Conferece on Thermal and Thermomechanical Phenomena in Electronnic Systems (ITherm), 2012, pp.1159-69.

Table caption

Table 1. Parameters used for modeling.

Figure captions

Fig. 1. Schematic diagrams of (a) an MCFC-TEG hybrid system and (b) a TEG.

Fig. 2. Comparisons of (a) power densities and (b) efficiencies between the MCFC, TEG, and hybrid system with the operating current density of the MCFC, where $P_{MCFC}^{*} = P_{MCFC} / A$, $P_{TEG}^{*} = P_{TEG} / A$, $P^{*} = P / A$ are, respectively, the corresponding power densities for the MCFC, TEG and hybrid system; $P_{MCFC,\max}^{*}$, $P_{TEG,\max}^{*}$ and $P_{\max}^{*}$ are, respectively, the maximum power densities for the MCFC, TEG and the hybrid system; j_P and η_P are, respectively, the operating current density and efficiency of the hybrid system at $P_{\max}^{*}$; $j_{P,fc}$ and $\eta_{P,fc}$ are, respectively, the operating current density and efficiency of the MCFC at $P_{MCFC,\max}^{*}$; $j_{P,t}$ is the operating current density at $P_{TEG,\max}^{*}$, $j_{\eta,t}$ is the operating current density at the maximum efficiency of the TEG $\eta_{TEG,\max}$; P_C^{*} and η_C are, respectively, the power density and efficiency of the hybrid system at j_C, and j_S is the stagnation current density from which the MCFC cannot output electrical power any more.

Fig. 3. Maximum power density improvement comparisons between some bottoming thermal devices for MCFCs.

Fig. 4. Effects of operating temperature T on the performance of the hybrid system.

Fig. 5. Effects of operating pressure P on the performance of the hybrid system.

Fig. 6. Effects of heat conductivity K on the performance of the hybrid system.

Fig. 7. Effects of coefficients c_1 and/or c_2 on the performance of the hybrid system.

Fig. 8. Effects of dimensional figure of merit of thermoelectric materials on the performance of the

hybrid system.

Table 1.

Parameter	Value
Faraday constant, F (C mol^{-1})	96,485
Number of electrons, n_e	2
Universal gas constant, R (J mol^{-1} K^{-1})	8.314
Operating temperature, T (K)	893
Operating pressure, p (atm)	1
Anode gas compositions	60%H_2/15%CO_2/25%H_2O [41]
Cathode gas compositions	59%N_2/8%O_2/8CO_2/25%H_2O [41]
Activation energy in the anode, $E_{act,an}$ (J mol^{-1})	53,500 [41]
Activation energy in the cathode, $E_{act,cat}$ (J mol^{-1})	77,300 [41]
Effective polar plate area of the MCFC, A (m^2)	0.011
Temperature of environment, T_0 (K)	298
Figure of merit of the semiconductor materials, ZT_0	1.0 [46]
Heat conductivity, K (W K^{-1} m^{-1})	0.02 [48]
Constant, c_1 (W K^{-1} m^{-2})	0.1 [50]
Constant, c_1 (W K^{-1} m^{-2})	0.1 [50]

Fig. 1.

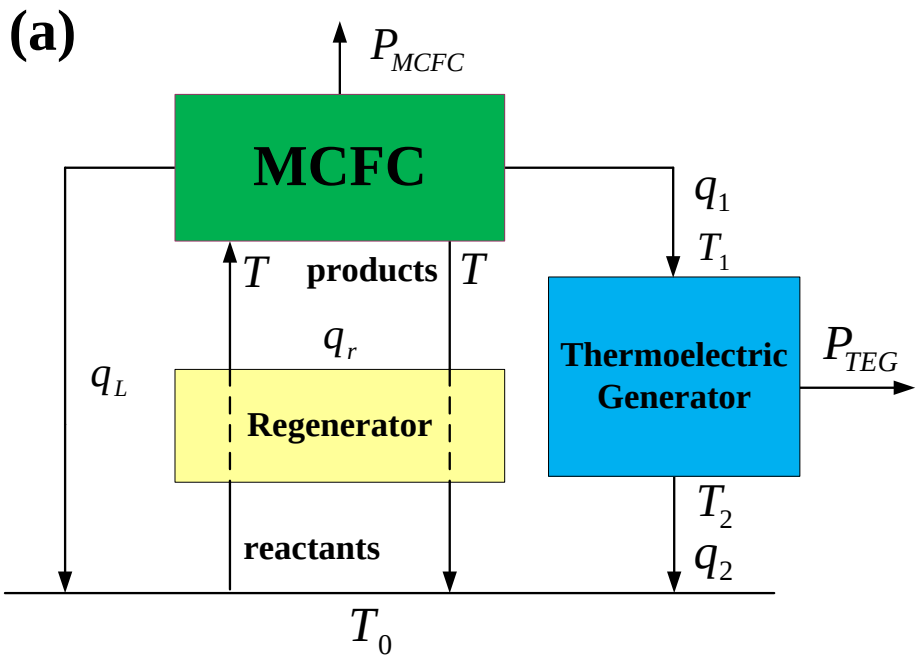
(a)
P_{MCFC}
MCFC
q_1
T_1
T
products
T
q_r
q_L
Regenerator
Thermoelectric Generator
P_{TEG}
T_2
reactants
q_2
T_0

(a)

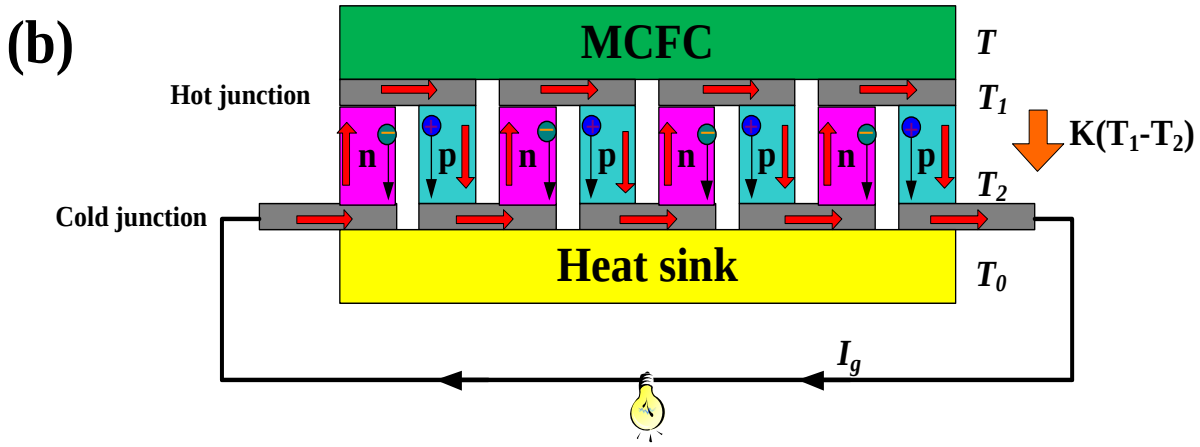
(b)
MCFC
T
Hot junction
T_1
K(T1-T2)
n
p
T_2
Cold junction
Heat sink
T_0
I_g

(b)

Fig. 2 (a).

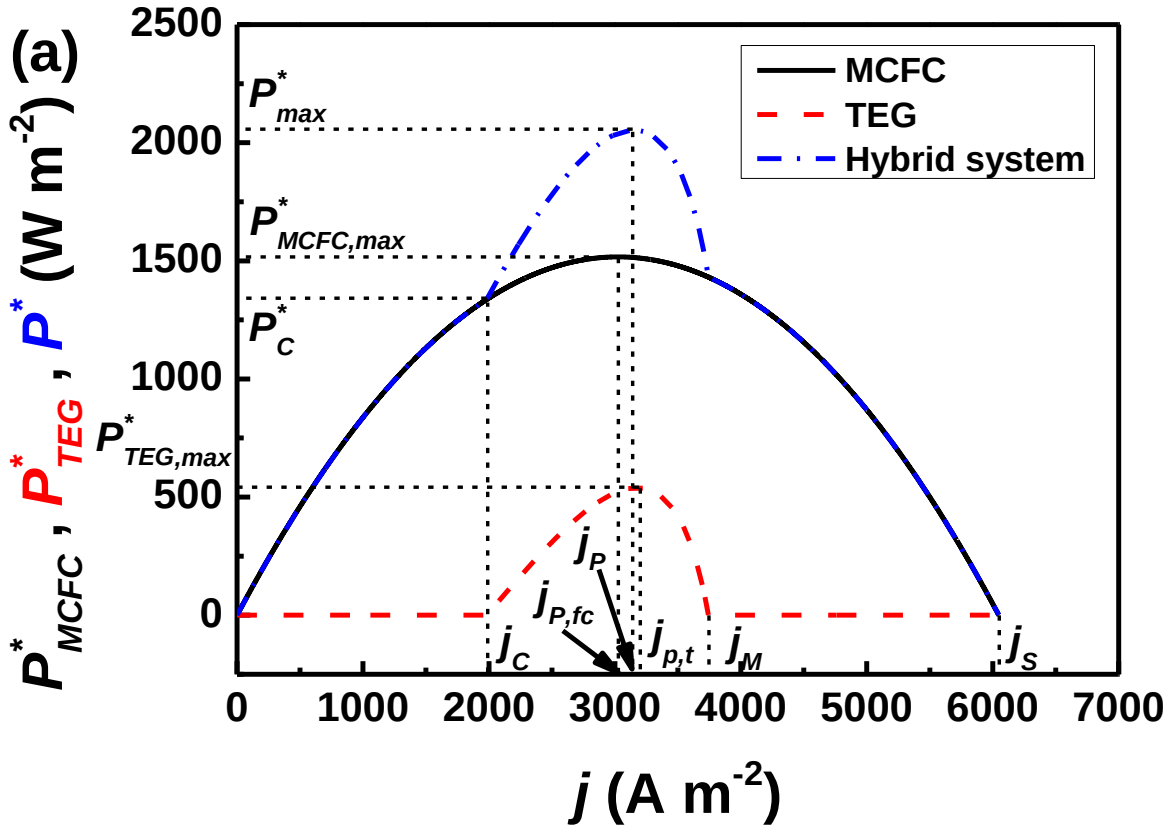
(a)
MCFC
TEG
Hybrid system
P^*_{max}
$P^*_{MCFC,max}$
P^*_C
$P^*_{TEG,max}$
j_P
$j_{P,fc}$
j_C
$j_{p,t}$
j_M
j_S
P^*_{MCFC} , P^*_{TEG} , P^* (W m^{-2})
j (A m^{-2})
2500
2000
1500
1000
500
0
0
1000
2000
3000
4000
5000
6000
7000

Fig. 2 (b).

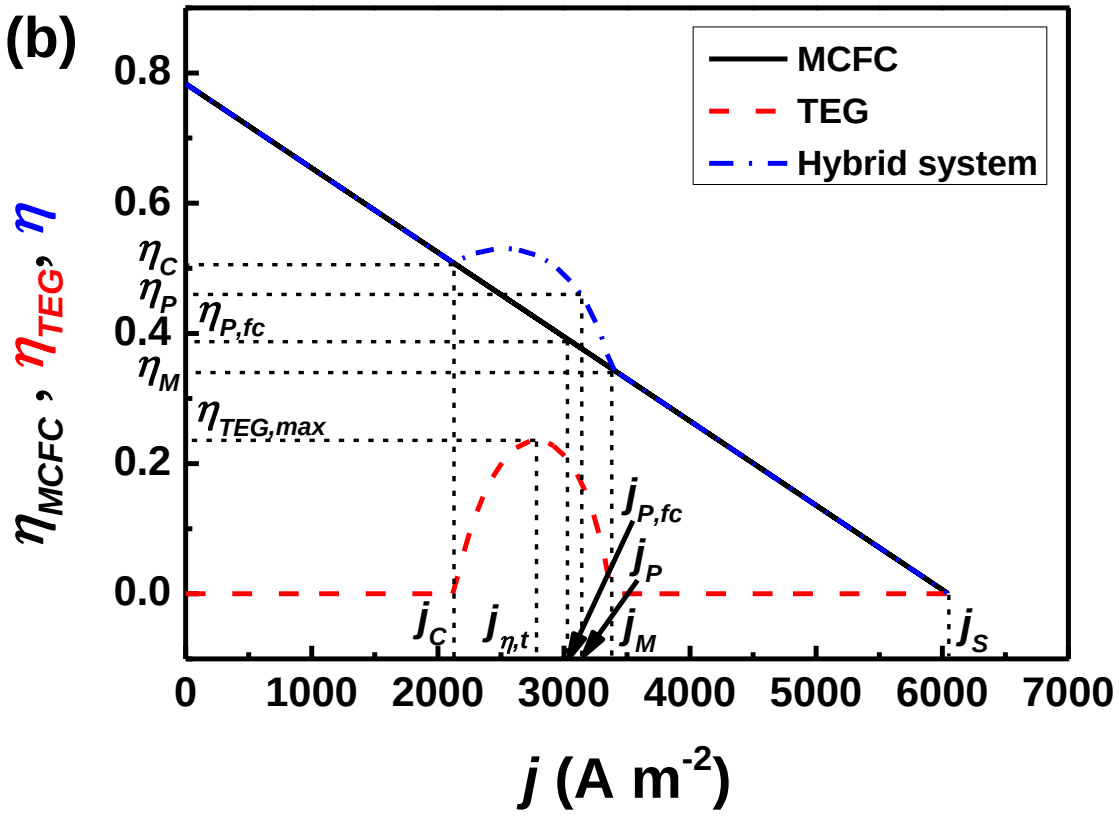
(b)
MCFC
TEG
Hybrid system
0.8
0.6
0.4
0.2
0.0
η_C
η_P
$\eta_{P,fc}$
η_M
$\eta_{TEG,max}$
η_{MCFC} , η_{TEG}, η
$j_{P,fc}$
j_P
j_C
$j_{\eta,t}$
j_M
j_S
0
1000
2000
3000
4000
5000
6000
7000
j (A m^{-2})

Fig. 3.

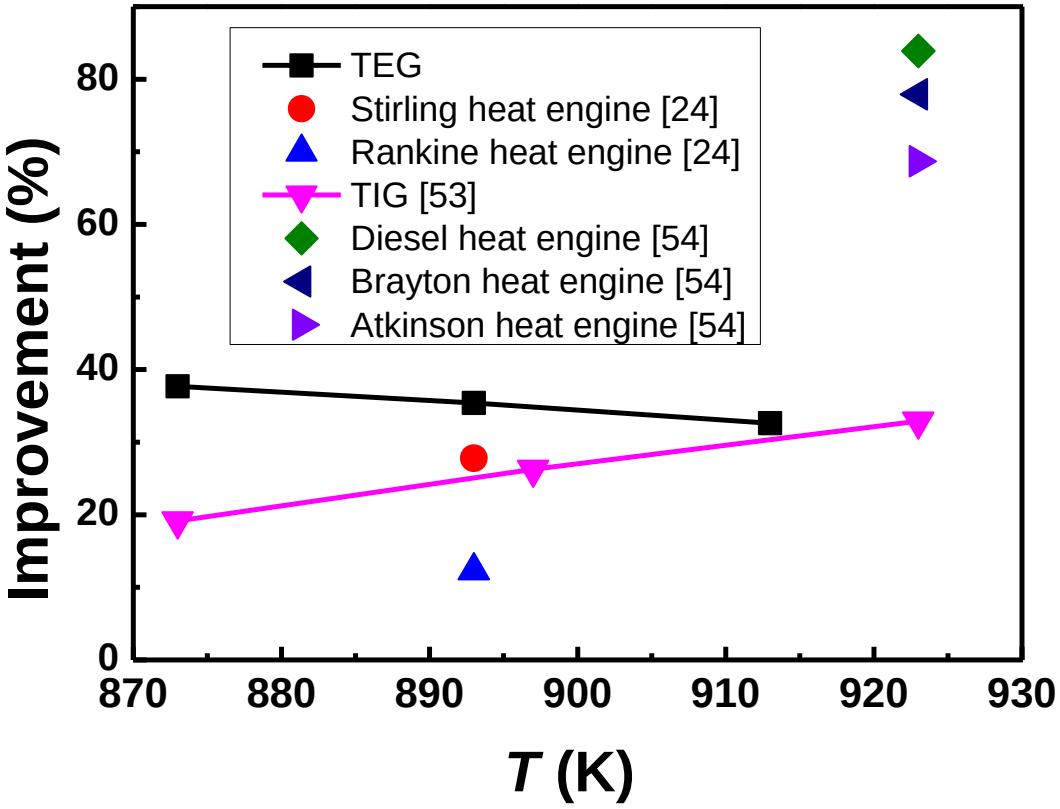
TEG
Stirling heat engine [24]
Rankine heat engine [24]
TIG [53]
Diesel heat engine [54]
Brayton heat engine [54]
Atkinson heat engine [54]
Improvement (%)
0
20
40
60
80
870
880
890
900
910
920
930
T (K)

Fig. 4.

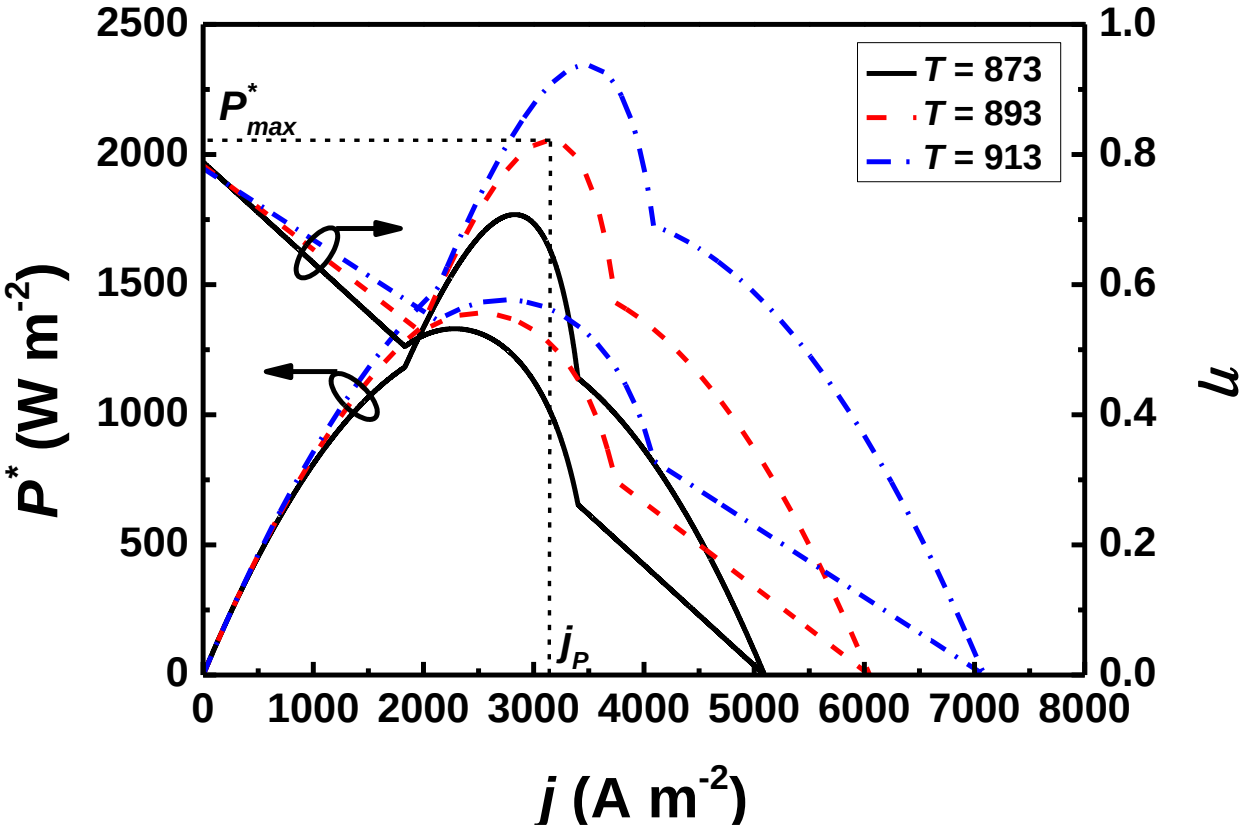
2500
2000
1500
1000
500
0
1.0
0.8
0.6
0.4
0.2
0.0
0
1000
2000
3000
4000
5000
6000
7000
8000
P* (W m-2)
u
j (A m-2)
P*max
jP
T = 873
T = 893
T = 913

Fig. 5.

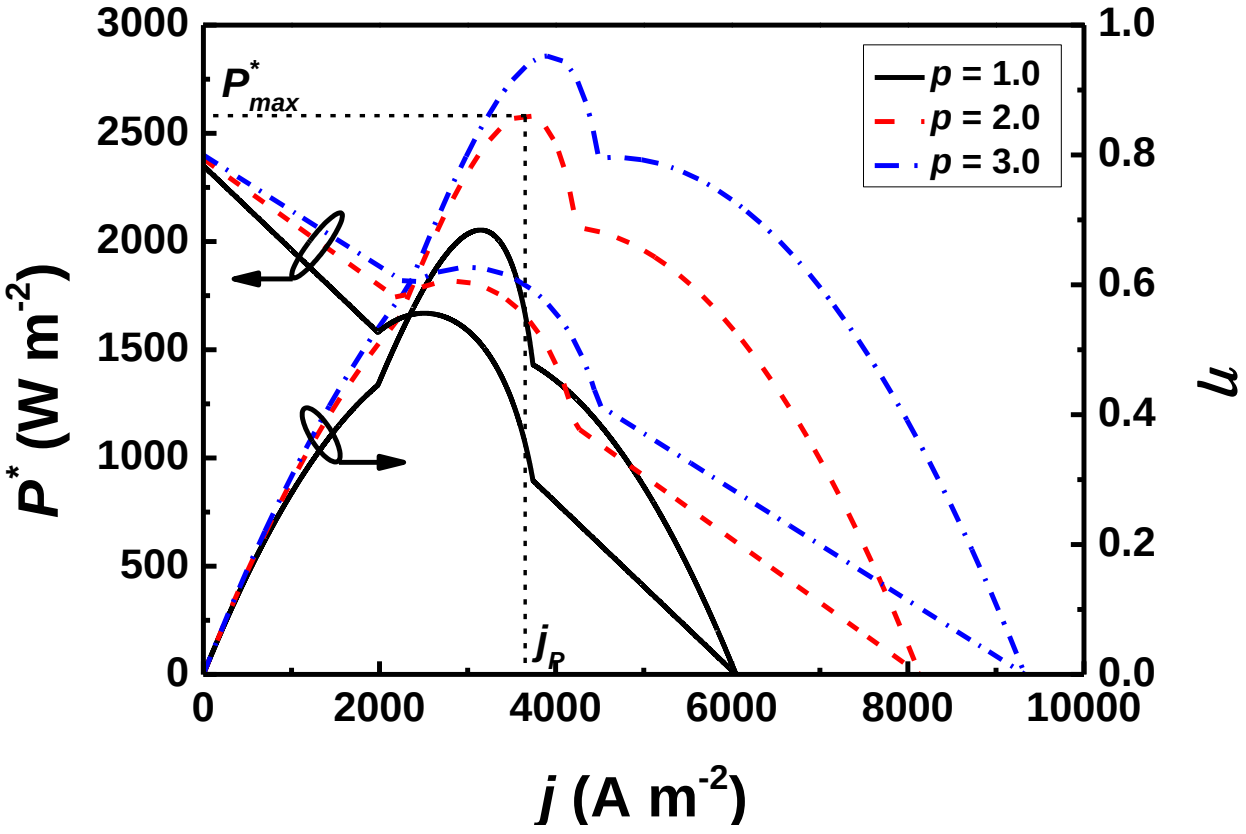
3000
2500
2000
1500
1000
500
0
1.0
0.8
0.6
0.4
0.2
0.0
0
2000
4000
6000
8000
10000
P*max
jP
p = 1.0
p = 2.0
p = 3.0
P* (W m-2)
u
j (A m-2)

Fig. 6.

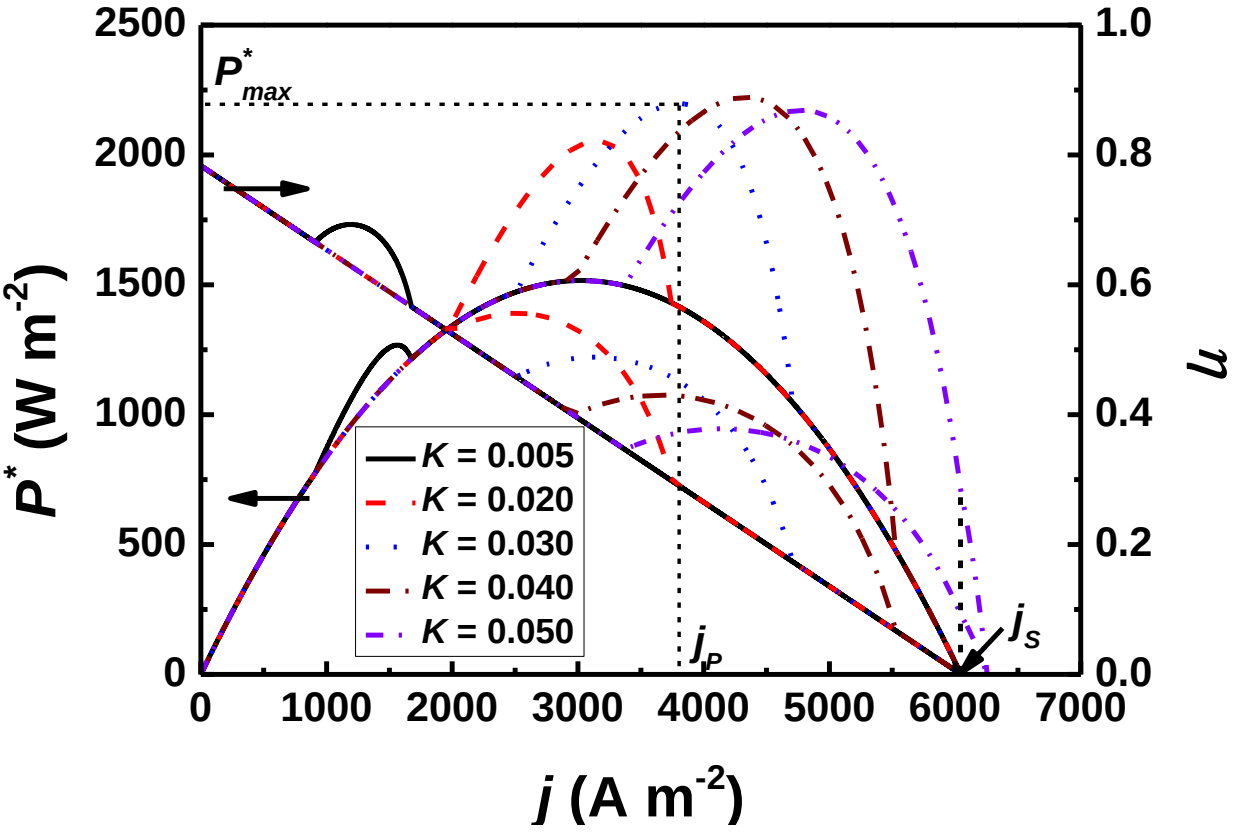
2500
2000
1500
1000
500
0
1.0
0.8
0.6
0.4
0.2
0.0
0
1000
2000
3000
4000
5000
6000
7000
P*max
P* (W m-2)
η
j (A m-2)
K = 0.005
K = 0.020
K = 0.030
K = 0.040
K = 0.050
jP
jS

Fig. 7.

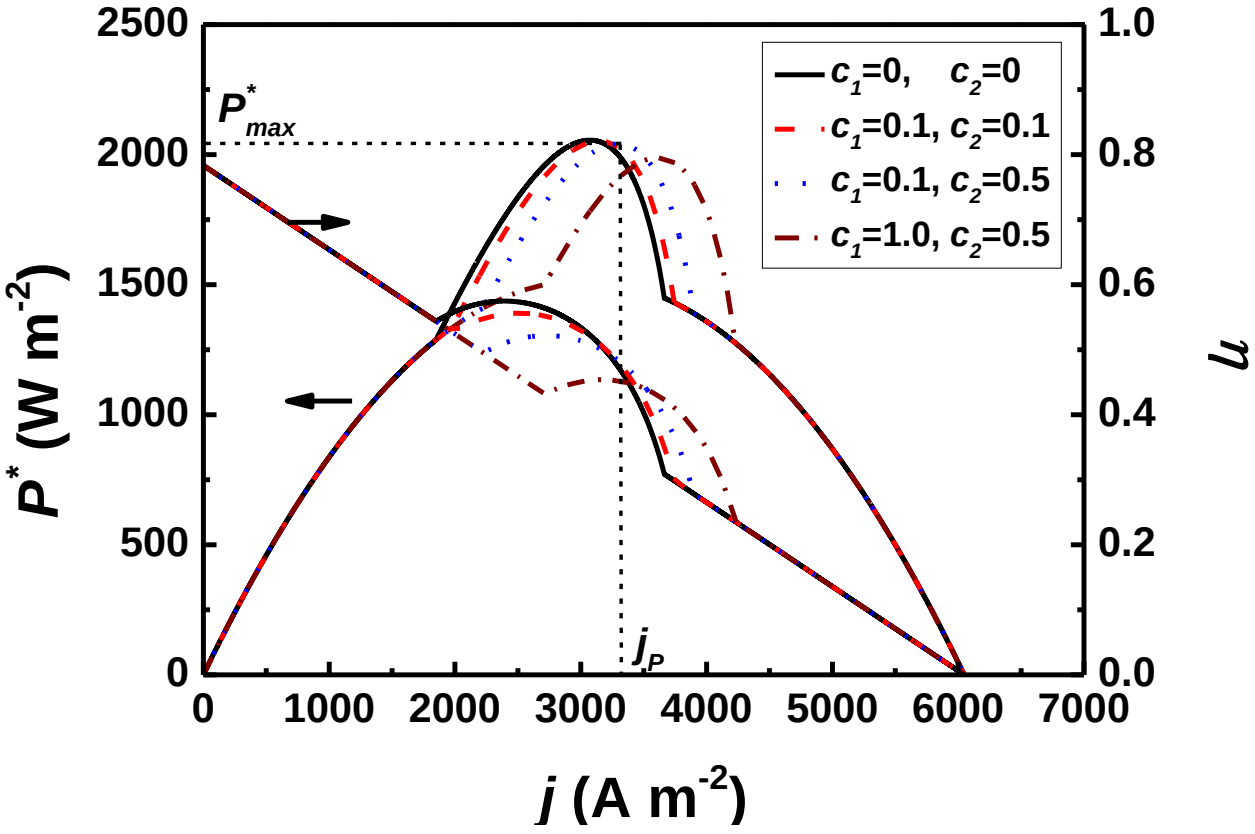
2500
2000
1500
1000
500
0
1.0
0.8
0.6
0.4
0.2
0.0
0
1000
2000
3000
4000
5000
6000
7000
P* (W m-2)
u
j (A m-2)
P*max
jP
c1=0, c2=0
c1=0.1, c2=0.1
c1=0.1, c2=0.5
c1=1.0, c2=0.5

Fig. 8.

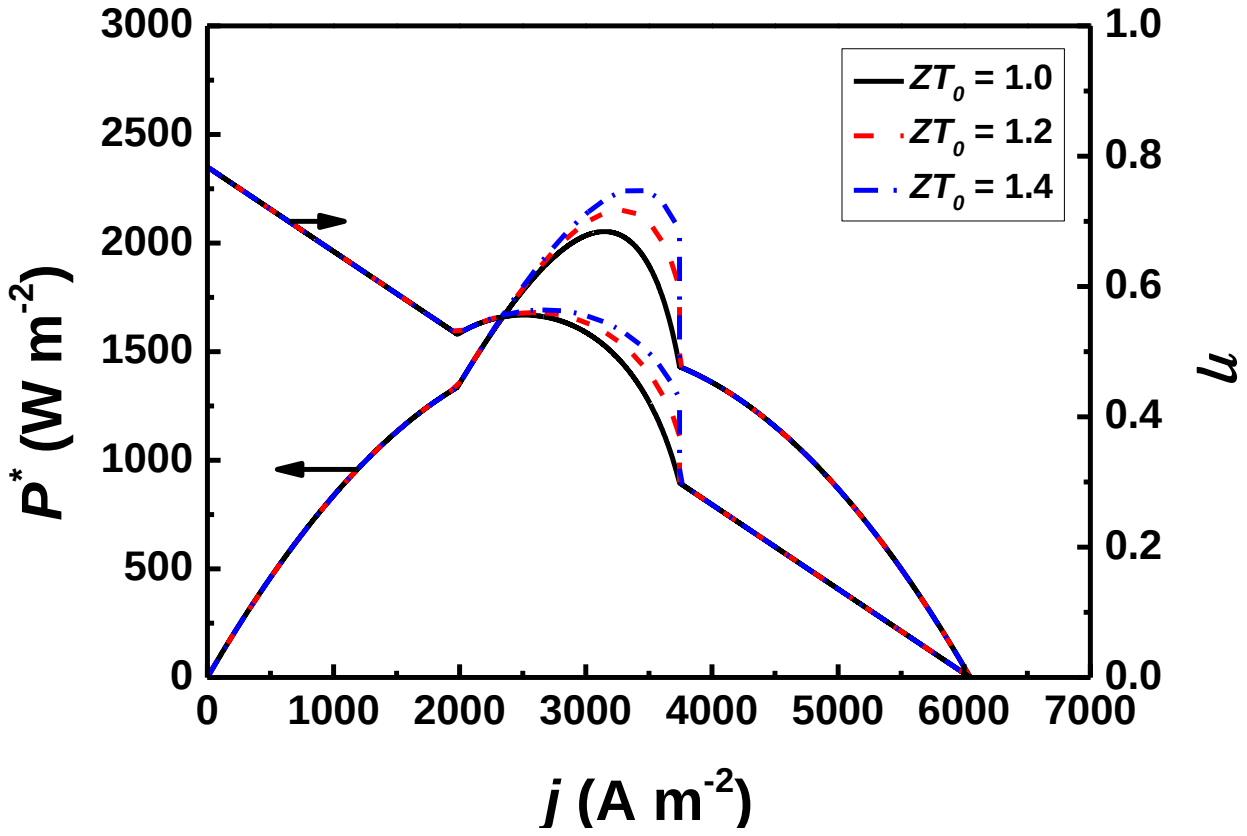
3000
2500
2000
1500
1000
500
0
1.0
0.8
0.6
0.4
0.2
0.0
0
1000
2000
3000
4000
5000
6000
7000
P^* (W m^{-2})
η
j (A m^{-2})
ZT_0 = 1.0
ZT_0 = 1.2
ZT_0 = 1.4